

Structure development during shear flow induced
crystallization of i-PP: in situ small angle x-ray
scattering study.

Rajesh H. Somani, Benjamin S. Hsiao*

Department of Chemistry, State University of New York

Stony Brook, NY 11974 - 3400

Srivatsan Srinivas, Andy H. Tsou

ExxonMobil Chemical Company, Baytown Polymers Center, TX 77522.

Igors Sics, Aurora Nogales, Francisco J. Balta-Calleja, Tiberio A. Ezquerra

Instituto de Estructura de la Materia, Madrid, Spain.

* - Author for correspondence.

Abstract

In-situ synchrotron small-angle x-ray scattering (SAXS) was used to follow orientation of isotactic polypropylene in the sub-cooled melt at 140 °C after step-shear under isothermal conditions. The melt was subjected to a shear strain of 1400% at three different shear rates (10, 57, and 102 s⁻¹) using a modified Linkam shear stage. The SAXS patterns show strong meridional reflections due to the rapid development of oriented polymer crystallites within the melt. Based on the SAXS data, a model for shear flow induced crystallization in isotactic polypropylene polymer is proposed. During flow extended microfibrillar structures develop parallel to the flow direction, enhancing nucleation of the folded chain crystals which grow perpendicularly to the flow direction. The half time of crystallization was calculated from the evolution profiles of the total scattered intensity. The crystallization kinetics increases by two orders of magnitude as compared to quiescent crystallization. A method was used to deconvolute the total integrated scattered intensity into the isotropic and anisotropic components of the crystallized polymer. The fraction of oriented crystallites in the bulk material was determined from the ratio of the scattered intensity due to the oriented crystallites (anisotropic component) to the total scattered intensity. At low shear rates (~ 10 s⁻¹) the oriented fraction in the polymer bulk was lower than at high shear rates (57, and 102 s⁻¹). It is shown that only the polymer molecules above a "critical orientation molecular weight" (M*) can become oriented at a given shear rate. The M* values at different shear rates were calculated from the area fractions of the molecular weight distribution

of polymer. The dependence of M^* on shear rate was estimated from the relationship, $M^* \sim \dot{\gamma}^{-\beta}$. Analysis of results suggests that the value of M^* is sensitive at low shear rates (below 60 s^{-1}). Experimental results are shown to be in agreement with theoretical predictions.

Introduction

In most polymer processing methods, such as extrusion, injection molding, fiber spinning, etc., the molten polymer is exposed to varying levels of flow-fields (elongation, shear, mixed) (1). In the 1970's a great effort was devoted to elucidate fiber formation under elongational flow from dilute polymer solutions (2-9). The study of fiber formation using elongational flow injection molding methods was later, also, object of interest (10-12). Shear flow was often neglected, as it was considered at that time as a "weak" flow, incapable to provide extension of polymer chains to induce further fiber formation at different stages of the process. However, in polymer melts even shear flow modifies the crystallization behavior and the resulting morphologies; shear flow accelerates, in fact, the overall kinetics (13 -20), and shish-kebab structures have been observed in the deformed polymer matrix (21). A summary of shear-induced crystallization studies has been compiled by Trobout (22).

It is known that polymer melts, under the influence of a shear field (rate, strain, and duration of shear), exhibit an increased rate of crystallization and a different morphology, when compared with quiescent melt (1-9). Kalay (23) reported that shear-controlled orientation injection molding (SCORIM) results in more pronounced orientation with a substantial increase in the Young's modulus of the final products produced. The improved mechanical properties of the SCORIM i-PP products were attributed to the shish-kebab morphology developed by the action of shear to the solidifying melt. Furthermore, Huang (24)

demonstrated that improved properties could be produced from continuous melt extrusion under controlled processing conditions for polypropylene. For example, self-reinforced i-PP sheets prepared at 172 °C and a die pressure of 40 MPa exhibited higher values of the melting temperature, tensile strength, and light transmittance than when prepared at 162 °C. This was attributed to a more developed highly oriented extended-chain crystalline structure of the former.

The crystallization process in polymers and the resulting morphology are strongly dependent on parameters such as processing temperature, applied shear (or elongation) rate, shear strain, and shear duration (ref.24^a). Molecular parameters, such as molecular weight, molecular weight distribution, chain branching etc., and the presence of nucleating agents play, as well, an important role. The structure of isotactic polypropylene reflects very accurately any changes in the aforementioned parameters (25). Several researchers have investigated the effects of shear (and elongation) fields on the crystalline morphology of isotactic polypropylene. Varga, et.al. (26) studied shear-induced crystallization of isotactic polypropylene and copolymers using a thermo-optical technique; concluding that melt-shearing causes the development of row-nuclei in the form of microfibril bundles. Row-nuclei generate the epitaxial growth of folded chain lamellae that fill the space normal (perpendicular) to the row-nuclei, resulting in a supermolecular structure of cylindric symmetry. The latter morphology was referred to as a cylindrite by Kargin et.al (27), and Binsenberg (28). Kornfield and coworkers (8) investigated the effects of short term shearing

on the subsequent crystallization of a polydisperse Ziegler-Natta isotactic polypropylene using *in-situ* optical and wide-angle x-ray diffraction (WAXD) measurements and *ex-situ* microscopy. *Ex-situ* optical and electron microscopy observations (9) of the polypropylene specimens quenched after shear crystallization reveal that the highly oriented crystallites develop in a row nucleated or shish-kebab morphology; the parent lamellae (kebab) growing radially from central line nuclei (shish) until they impinge with each other.

According to Thomason and Van Rooyen (29) a low level of applied stress is sufficient to create a shear-induced layer in a Twaron aramid fiber/PP system. These authors observed two distinct morphologies in the melt-undergoing shear: bulk spherulites and a shear-induced layer. Misra, et.al. (30) studied the role of molecular weight distribution on the spinnability, structure, and properties of melt-spun isotactic polypropylene filaments. Vleeshouwers and Meijer (31) reported the influence of shear on isothermal crystallization of isotactic polypropylene of different molecular weight and distribution. Shear rate and time revealed independent influences on crystallization. Short times at high rates were found to be most effective. Furthermore, it was shown that the crystallization behavior is very sensitive to molecular weight and distribution. Moitzi and Skalicky (32) indicate that even a small shearing of the melt, after a few seconds, enhances the crystallization of isotactic polypropylene at 130 and 135 °C. In a recent study (33), Haudin and Monasse, measured the crystallization kinetics of polypropylenes with various molecular weights during shear experiments in a

fiber-pullout device. They observed that the crystallization sensitivity of a given polypropylene to shear depends on its molecular weight.

The quantitative evaluation of the shear-field effects is at present hampered by the difficulty in the description of the crystal morphology and molecular conformation of crystals grown from a deformed melt (34). Very few *in-situ* measurements are concerned with the nuclei formed under shear and the growth rate of the subsequent morphologies (29). The combination of high shear rate and short-term shearing with subsequent monitoring of the structure development occurring in the melt has been tried only recently by Jerschow and Janeschitz-Kriegl (35). Kornfield and coworkers (8,9) have recently studied the influence of short term shearing using *both in-situ* optical (birefringence) and wide-angle x-ray diffraction (WAXD), and *ex-situ* microscopy techniques.

Step shear deformation experiments on i-PP using *in-situ* SAXS have not been reported before in the literature. The aim of the present study is thus to extend the above investigations to the study of the structure development of isotactic polypropylene in the undercooled melt (at 140 °C) subjected to a brief impulse of step shear (with high shear rate and high strain) using *in-situ* synchrotron small-angle x-ray scattering (SAXS). It will be shown that the combination of high shear rate (similar to polymer processing operations) and high strain orients the polymer molecules in the melt preferentially in the flow direction. The present results additionally highlight the fact that the imposed

shear field affects the extent of molecular orientation in the melt and the final resulting crystalline morphology. An attempt to estimate the fraction of oriented species in the bulk polymer is made from the SAXS data taken at different shear rates. Finally a "critical orientation molecular weight" (M^*), defining the molecules above a chain length that become oriented at a given shear rate, is introduced.

Experimental

Materials

Ziegler-Natta isotactic polypropylene homopolymer (i-PP) supplied by ExxonMobil Chemical Company was used in this study. The molecular weights of the i-PP resin, as obtained from the GPC experiments, were $M_n = 92,203$, $M_w = 368,935$, and $M_z = 964,632$. Polymer films of 0.5 to 1.0 mm thickness were prepared in a laboratory press at 200 °C. Samples in the form of a ring (ID = 10mm, OD = 20 mm) were cut from the molded films for the x-ray scattering measurements.

Techniques

Shear stage

A Linkam CSS-450 high temperature shearing stage modified for application in x-ray scattering '*in-situ*' studies was used to precisely control shear-field and thermal history of the polymer sample. Kapton windows were used in place of the standard quartz optical windows on the top and bottom steel blocks

(two parallel plates) of the Linkam stage (Figure 1). The top plate has a narrow aperture hole ($d = 3 \text{ mm}$), which allows the x-ray beam ($d = 0.9 \text{ mm}$) to enter the sample. The bottom plate, which is also the rotating plate, has three open slots (wider than the hole in the top window). Thin kapton films were glued to the surfaces of the top and bottom plates, the latter serving as the actual x-ray window material. The sample is held in the gap between the two windows and is sheared by rotating the bottom plate by a precision stepping motor, while the top plate remains stationary. The open slots in the bottom window allow the scattered x-ray beam to pass directly through the sheared sample. The windows fit together in such a way that the sample is sealed. Polymer melts are fairly viscous and no leakage is detected even when the Linkam stage is mounted in the vertical position (necessary since the x-ray beam travels horizontally). The mechanical design and electronics of the Linkam stage provides a precise control of various parameters of the shear experiment. These include, temperature, heating/cooling rates, sample thickness, shear strain, shear rate, and shear duration as well as shear mode, step, steady, and oscillatory. The shearing stage is compact and can be easily setup for in-situ x-ray scattering experiments in a synchrotron beamline.

In all our experiments the step shear mode was selected. The shear rate and strain conditions were chosen in such a way that the bottom window would rotate less than a one full circle (360°). The advantage of the step shear mode is that the polymer melt is deformed only once, as compared to the steady shear

in which the fluid elements rotate as well as undergo shear. The strain rate will in the steady shear change sign periodically (34). The total strain and the strain rate cannot be varied independently in steady shear flow and experiments cannot be conclusive as to whether a strain rate or a total strain requirement is pertinent to the onset of fibrous crystallization in flowing melts. Keller and Kolnaar (3) pointed out the need for an experimental setup where the strain rate and the total strain can be varied independently. The step shear mode in the Linkam shear stage provides such a set-up in which the shear parameters (shear rate and % strain) can be varied independently.

The above-described arrangement gives a parallel-plate shearing geometry. The shear profile across the thickness of the polymer sample is schematically shown in Figure 2. The polymer molecules at the surface of the bottom plate (rotating plate) undergo the maximum shear, which decreases linearly to a zero value at the surface of the top plate (stationary plate). Thus the molecules should show a maximum degree of orientation near the maximum shear surface gradually decreasing across the sample thickness. The resultant morphology in the polymer bulk is expected to have a "skin-core" type of structure, similar to the structures observed in the extrusion and injection molding polymers.

Small Angle X-ray Scattering measurements

SAXS measurements were carried out at the Advanced Polymers Beamline (X27C, $\lambda = 1.307 \text{ \AA}$) in the National Synchrotron Light Source (NSLS), Brookhaven National Laboratory (BNL). A 3-pinhole collimator system was used for beam alignment. A 2D MAR CCD x-ray detector (MARUSA) was employed for the detection of 2D SAXS images having a resolution of 512×512 pixels (pixel size = $257.6 \text{ }\mu\text{m}$). The sample to detector distance was 1740 mm. The schematics illustrating the SAXS setup is presented in Figure 1.

Experimental procedure

In each experiment, the polymer sample (in the form of a ring) was mounted between the two x-ray windows. The gap between the two windows was set equal to the sample thickness. In order to ensure that the polymer melt was free of any memory effects associated with clusters, crystal aggregates and molecular conformation due to temperature and deformation history, all samples were subjected to the same thermal history, as shown in Figure 3. The temperature control program for the shear stage was set as follows:

- 1) Heating at a rate of $10 \text{ }^\circ\text{C}/\text{min}$ from room temperature to $210 \text{ }^\circ\text{C}$.
- 2) Hold the temperature at $210 \text{ }^\circ\text{C}$ for 5 min.
- 3) Cooling at a rate of $30 \text{ }^\circ\text{C}/\text{min}$ down to $140 \text{ }^\circ\text{C}$ to carry out x-ray measurements.
- 4) Hold the temperature at $140 \text{ }^\circ\text{C}$ for 30 min.

A crystallization temperature of 140 °C was chosen so that the nucleation and crystal growth times are relatively long under quiescent conditions. Half time of crystallization under quiescent conditions for polypropylene at this temperature is $\sim 10^4$ s (27). Hence, the observed changes in the crystallization kinetics at 140 °C after shear can be attributed to the imposed shear conditions.

Two-dimensional SAXS images were taken immediately after the polymer reaches 140 °C. The data acquisition time for each scattering pattern (image) was 10 s, with an interval of 5 s between adjacent images. Typically 100 SAXS images were collected in a single run. After collection of three images where no shear was present, the polymer melt was subjected to a brief impulse of step shear from time $t = 0$ to t_s (Figure 3). The step shear conditions were also monitored by a CCD camera. Three different shear rates, 10, 57, and 102 s^{-1} were used. A high strain value of 1428% was used in all our experiments. Thus, the duration of the step shear was 1.4, 0.25, 0.14 s corresponding to the shear rates of 10, 57, and 102 s^{-1} respectively. The SAXS images were collected continuously; before, during, and after cessation of the applied shear. Since the shear rate decreases linearly across the thickness of the sample to a minimum value at the top surface (Figure 2) the scattering images represent the average of the scattered intensity from the scatterers across the thickness of the sample.

An air scattering pattern (10 s acquisition time) at the temperature of 140 °C with no sample between the two windows of the shear stage was also

collected. The air scattering pattern was used for the background correction of the scattering images of the polypropylene samples; X-ray data was also normalized for sample thickness. Subsequent analysis of the x-ray data was carried out on the corrected and normalized scattering patterns.

Results

SAXS Patterns

Figure 4 illustrates the representative two-dimensional SAXS patterns of the polypropylene sample at 140 °C before and after application of a step shear (102 s^{-1} shear rate and 1428% strain). The pattern of the initial amorphous melt (Figure 4a) consists of a diffuse ring from the isotropic melt indicating the absence of any detectable structures and/or preferred orientation. This pattern is observed before shear in all experiments, confirming thermal clearing of any memory effects in the polypropylene melt.

Figure 4b shows the scattering pattern obtained 120 s after the applied shear (duration of the shear was 0.14 s). The pattern clearly shows the appearance of meridional maxima from the oriented scatterers (growing lamellae in the melt). It should be noted that the discrete reflections were observed almost immediately after the shear pulse was applied. The data acquisition time for each image was 10 s and already the first image collected after shear shows discrete reflections. Thus, the oriented structures clearly develop immediately after the application of the brief pulse of the step shear. The intensity of discrete

reflections in the consecutive images becomes gradually stronger, due to the growth of crystalline structures in the melt. Furthermore, the azimuthal breadth becomes broader owing to the decrease in orientation. After certain time, the intensity of the discrete reflections remains constant and no significant change was observed anymore in the scattering pattern. Figure 4c shows the scattering image of the sample 900 s after the applied shear. Here the oriented SAXS maxima are better defined, though they appear superimposed to an isotropic scattering ring.

Analysis of the SAXS Data

In each experiment, at least 100 images of the SAXS patterns were collected, starting with the completely amorphous melt at 140 °C (before shear), during shear, and after cessation of shear. The time period between each image was 15 seconds. The SAXS image at time $t = 0$ corresponds to the amorphous melt. In all experiments, the SAXS image at $t = 15$ s shows the discrete reflections (although weaker in intensity) due to the growth of the oriented crystalline lamellae in the melt. The melt crystallizes completely, in few minutes, as evidenced by no change in the SAXS pattern thereafter.

The integrated (or total) scattered intensity of each SAXS pattern is due to the contribution of all the scatterers in the polymer sample. Initially, at $t = 0$, there are very few scattering species (or scatterers) in the polymer melt and the integrated intensity is, consequently, low. Owing to the imposed step shear, the

polymer molecules orient in the flow direction and form a highly oriented "shear-induced structure" (8,9). This "shear-induced structure" provides the nucleation sites for the crystallites that grow after cessation of shear. However it has been reported that the lamellar thickness', cross-hatching frequencies and growth rates are independent of the type of nucleation; point, surface or row-nucleated (36). Thus, the growth of both the oriented crystallites as well as the randomly distributed crystallites is expected to occur in the fast crystallizing melt after cessation of the shear. The resultant morphology of the polymer bulk consists of both; the preferentially oriented crystalline lamellae and randomly distributed lamellae.

The total scattered intensity ($I_{\text{total}}[s, \phi]$), from the polymer sample has two components, 1) $I_{\text{unoriented}}[s]$, which is due to the scattering from the randomly distributed crystalline lamellae (scatterers) and 2) $I_{\text{oriented}}[s, \phi]$, originated by the scattering from oriented lamellae. The total scattered intensity can be represented as follows:

$$I_{\text{total}}[s, \phi] = I_{\text{unoriented}}[s] + I_{\text{oriented}}[s, \phi] \quad (1)$$

where, $s = 2\sin\theta/\lambda$ is the scattering vector, 2θ the scattering angle, and ϕ the azimuthal angle.

The two components of the total scattered intensity can be deconvoluted into the contributions from the individual components. The scattered intensity arising from the unoriented scatterers (isotropic) is azimuthal independent, while

the scattering arising from the oriented scatterers is azimuthal dependent. The scattering from the unoriented component includes the amorphous phase and the Compton scattering from the chemical structure which is small (especially at low angles) and may be ignored. The isotropic component of the total intensity, $I_{\text{unoriented}}$, can be obtained from the "Halo" method (37). Accordingly, a series of the azimuthal scans were drawn along the scattering vector (or the angular axes 2θ) starting from the center of the diffraction pattern. At each angular pixel position, a minimum scattering intensity value can be obtained from the corresponding azimuthal scan. Thus, a series of the minimum scattering intensity values are obtained from the azimuthal scans along the angular axes. The minimum intensity can be, then, attributed to the isotropic scatterers and variations in the intensity at a particular azimuth can be assigned to the presence of preferentially oriented scatterers. The intensity envelope obtained from the series of the minimum values represents contribution from the unoriented scatterers.

The analytical procedure is further explained in Figure 5, showing the 2D SAXS image of the total scattered intensity pattern (A frame 300s after shear is shown in the example, Figure 5a). Figure 5b shows the 2D image of the calculated isotropic intensity pattern (from the "Halo" method). The pattern clearly shows the series of iso-intensity rings, similar to the scattering pattern of crystallites in an undeformed polymer sample. The constant intensity rings originate from the random distribution of the crystallites without any preferred

orientation in the polymer bulk. Figure 5c shows the 2D image obtained after subtraction of the image corresponding to the isotropic component from the total scattered intensity image (image 5b subtracted from image 5a). The strong scattered intensity envelope on the meridian of the SAXS pattern from the oriented scatterers can be clearly seen in Figure 5c.

The time evolution of the total scattered intensity, the azimuthal independent component, and the intensity due to the oriented scatterers are presented in Figure 6. The total scattering intensity rises very rapidly after the application of shear pulse; nearly a sudden intensity increase can be clearly seen in curve A. The integrated intensity reaches a plateau shortly thereafter, indicating the completion of the crystallization of the polymer melt. The azimuthal independent component of the total scattered intensity (curve B) has a low initial value (as one would expect, absence of the random scatterers) and, therefore, a very small contribution to the total scattered intensity. At this time the azimuthal independent scattering (that is, amorphous halo) is primarily due to the melt. As the randomly distributed crystallites grow in the melt, the scattered intensity increases, and as in the case of total scattered intensity curve it reaches the steady state value at the end of crystallization. On the other hand the scattered intensity ascribed to the oriented crystallites in the melt has a much higher contribution to the total scattered intensity at the beginning, that is, immediately after shear (curve C). In conclusion, the contribution of the oriented component

increases as the oriented crystals grow and reaches a steady value at the end of crystallization, as in the other two cases (curve A and B).

Effect of shear rate

Shear rate is, obviously, one of the most important parameters in the shear-induced crystallization of the polymer melt. The shear rate (and shear stress) must be high enough to orient and align the polymer macromolecules in the melt to form stable microfibril bundles (row-nuclei) in the flow direction. The stability of the oriented shear-induced structures formed after the application of the shear fields depends on the relaxation behavior of the polymer molecules in the melt. The longer chain molecules take a longer time for relaxation from deformation than the short ones. In a polymer with a broad distribution of the molecular weights (chain lengths), the longer chains from the high molecular weight tail give admittedly rise to "row-nuclei" due to a greater entanglement density and to a higher orientation than do the shorter chains. The short chain molecules relax in a very short time after deformation and hence cannot form row-nuclei. The extent of orientation of the polymer molecules, and the stability of the resulting oriented structures (row-nuclei) depend on, both, the level of the deformation (strain) and on the deformation rate (shear rate or elongation rate). At low strain levels (and high shear rate) the entangled polymer molecules cannot align and form the row-nuclei. At low shear rate (and high strain) levels the oriented molecules have sufficient time to relax and the stable row-nuclei cannot be formed. Thus, the higher values of the oriented fraction in the polymer

bulk crystallized after deformation are expected to be higher at high shear rates than the values of the oriented fraction at low shear rates. The time of crystallization for the polymer melt after deformation is also strongly influenced by the enhanced nucleation (due to row-nuclei) and the growth of the crystallites. Figure 7 illustrates the effect of shear rate on, both, the oriented fraction and the half time of crystallization for the i-PP sample at 140 °C. As expected, at low shear rates (10 s⁻¹), the oriented fraction is lower than the values at high shear rates (57, and 102 s⁻¹). At low shear rate (10 s⁻¹) the corresponding half time of crystallization is higher than at high shear rates (57, 102 s⁻¹). It should be noted that the crystallization times for i-PP at 140°C are still much lower, 525 s at 10s⁻¹, compared to ~ 10⁴ s under the quiescent crystallization conditions (i.e. near two orders of magnitude change). Unexpectedly the data from Figure 7 reveal that the oriented fraction as well as the half time of crystallization do not show a significant change when the shear rate is increased from 57 to 102 s⁻¹.

Discussion

Structure Development

The discrete meridional reflections in the SAXS patterns (along the shear direction) can be ascribed to the periodic arrangement of the crystal lamellae in the matrix. Application of Bragg's equation to the discrete reflection leads to the long spacing L , whereas the intensity distribution is a product of lamellar population and orientation. In oriented polymeric materials; such as spun fibers, biaxially oriented films, etc., the packing of the lamellae within the microfibrils

with respect to the draw direction account for the discrete reflections of varying intensity in the SAXS pattern. The preferential orientation of crystal lamellae, in the deformation or flow direction, results in an increase of intensity on the equator of the SAXS pattern. On the other hand the orientation of crystal lamellae perpendicularly to the flow direction results in an intensity increase on the meridian. The intensity and the azimuthal breadth of the equatorial and meridional scattering peaks are the measure of the number and orientation of scatterers in the polymer sample.

The intensity of the discrete reflections observed in the SAXS patterns obtained after cessation of step shear is strong in the meridian of the pattern (vertical) and are indicative of the preferential orientation of scatterers (crystal lamellae) perpendicularly to the flow direction. Let us recall that the flow direction in the sheared melt is not strictly vertical but it is tangential to the rotating movement of the bottom plate. This gives a slightly angular tilt to the meridional reflections on the SAXS patterns. Under the conditions used for the SAXS experiment discrete reflections were not observed in the equator of SAXS pattern. However, it is expected that upon application of the shear, the polymer molecules in the melt extend in the direction of shear field and form extended microfibrillar structures. This hypothesis is based on the observations of Goschel, et.al. (38), as well as of Kornfield and coworkers (8,9). Goschel, et.al. investigated the crystal growth and crystalline orientation in isotactic polypropylene at relatively high temperatures (159 to 170 °C) as a consequence

of flow-induced chain orientation in the melt using 2D WAXD. At high shear rates, 127.1 s^{-1} , strong equatorial reflections were observed indicating a preferential orientation of the crystallites in flow direction. Kornfield and coworkers (8,9) investigated the effects of short term shearing on the subsequent crystallization of a polydisperse Ziegler-Natta isotactic polypropylene using *in-situ* optical and WAXD measurements as well as *ex-situ* microscopy. During the shear pulse, they observed the generation of long-lived, highly oriented structures called "shear-induced structure" (from transient birefringence experiments). After cessation of flow, growth of the oriented crystallites off the "threadlike precursors" was observed, which resulted in the oriented morphology in the polypropylene sample. The low concentration and the large spatial distance ($> 1000 \text{ \AA}$, which is the detection limit of our SAXS instrument) between the microfibril structures formed in the polymer bulk under the conditions of the step shear used might explain the absence of an equatorial scattering in the SAXS patterns. Thus, we speculate that after the application of the step shear the long chain molecules orient in the flow direction, and that the oriented molecules form microfibrillar structures (shish) which provide nucleation sites for the subsequent crystal growth. The crystalline lamellae (kebabs) then grow radially from the nucleation lines, perpendicularly to the flow direction. The meridional reflections observed in the SAXS patterns immediately after the brief pulse of the step shear are, hence, due to the instantaneous formation and further growth of the lamellae oriented perpendicularly to the flow direction.

Based on our observations of the SAXS patterns and on the foregoing discussion we propose the following microstructural model for the crystallizing polymer after step shear (see Figure 8). Figure 8a schematically illustrates the random distribution of polymer molecules in the melt in various random conformations, before shear, with absence of preferred orientation. After step shear (<100 s) (Figure 8b), the long chain (high molecular weight) species orient preferentially in the flow direction. A “bundle” of long stretched molecules represents the row like “microfibril” structure in the melt due to the step shear (see Figure 8b). (Such a structure may develop into extended chain crystals, under conditions of very high shear rate and strain). This microfibrillar structure provides nucleation sites on which folded chain lamellae can grow radially outward in the perpendicular direction to the fibril axis. Randomly distributed crystalline lamellae, and less oriented lamellae (such as the daughter lamellae grown out of the parent ones), which grow in the polymer bulk simultaneously with the oriented lamellae are also shown in Figure 8b.

The oriented lamella are depicted farther apart at the beginning to indicate a large value of long spacing, which then decreases as new lamella grow from the other nuclei. Crystallization proceeds by means of further growth and insertion of both the oriented and unoriented crystalline lamella to fill the bulk of the polymer melt. Figure 8c schematically depicts the morphology of the fully crystallized polymer showing the row-nucleated structures (shish-kebab) as well as the unoriented lamellae.

Fraction of oriented material

Let us assume, in what follows, that the azimuthally dependent ($I_{\text{oriented}}[s,\phi]$) component of the total scattered intensity is directly proportional to the oriented fraction of the material in the polymer matrix. In this case, we ignore the question of the degree of orientation, but only address the issue of the fraction of the scatterers that are oriented. Based on the assumptions above, we can calculate the oriented fraction of the polymer material from the integrated scattered intensity values. The oriented fraction can be defined as the ratio of the scattered intensity due to oriented scatterers to the total scattered intensity. Figure 9 shows the calculated values of the oriented fraction as a function of time for the isotactic polypropylene sample at 140 °C, before and after the application of step shear (102 s⁻¹ shear rate and 1428% strain). In the ideal case, before shear there are zero oriented scatterers in the polymer melt. The crystallites grow immediately after shear. These are primarily oriented crystalline structures due to the applied shear. The rest of the bulk polymer has limited scatterers and, hence, the contribution of the unoriented scatterers to the total intensity is rather small. The fraction of oriented material immediately after shear is, therefore, very large. The unoriented scatterers grow as the polymer crystallization progresses and the concentration of the unoriented species as well as its contribution to the total scattered intensity increase more rapidly than the row-nucleated oriented species after cessation of shear. Therefore, the oriented fraction of the material decreases as a function of time after cessation of shear and reaches a steady value. The calculated value of the fraction of oriented material in the i-PP sample

after application of the step shear (102 s^{-1} shear rate and 1428% strain) at $140 \text{ }^{\circ}\text{C}$ is about 30%.

Half-time of crystallization

The half time of crystallization for isotactic polypropylene at $140 \text{ }^{\circ}\text{C}$ under different conditions of shear field; i.e, shear rates of 10, 57, and 102 s^{-1} were calculated from the total scattered intensity profiles. At $t = 0$ the value of the total scattered intensity, $I(0)$, is due to the amorphous, non-crystalline melt. The increase in the total scattered intensity, $I(t) - I(0)$, is, then, directly proportional to the growth of the crystallites in the bulk polymer. The total scattered intensity reaches a plateau, $I(s)$ (steady state value) at the end of the crystallization process. The fraction of crystallized material, X_c , was calculated as,

$$X_c = [I(t) - I(0)] / [I(s) - I(0)] \quad (2)$$

Figure 10 shows the time evolution profile of X_c for the i-PP sample at $140 \text{ }^{\circ}\text{C}$ after application of the step shear using a shear rate of 10 s^{-1} and 1428% strain.

The half time of crystallization was taken as the time corresponding to $X_c = 0.5$. At 10 s^{-1} shear rate, the half time of crystallization for the i-PP sample at $140 \text{ }^{\circ}\text{C}$ is 525 s.

Critical orientation molecular weight

The above results concerning the effect of shear rate can be explained if one considers the mechanism of the flow-induced crystallization at a molecular level. The major factor governing overall motion of polymer molecules in a polymer melt is the influence of the entanglements. In the quiescent state entanglements are created and removed through Brownian motion. Deformation or flow affect the number of entanglements. Hence, the entanglement density will be determined by the rate of deformation and the total strain imposed. At low rates a polymer melt will display high resistance to flow, i.e., high viscosity or high entanglement density. At higher rates of deformation the fluidity of the melt is enhanced (shear thinning) and the entanglement density is reduced. For flow induced crystallization, a certain degree of molecular extension must be achieved. When the time scale of straining is long relative to the time scale of disentanglement, orientation relaxation will occur prior to the achievement of a sufficient degree of molecular extension for nucleation to be feasible. Thus, both, a minimum strain and strain rate values have to be present for shear flow to induce crystallization. In order to crystallize a polymer melt at a given temperature and shear rate, the shear-induced crystallization effects are found to be critical in relation to the molecular weight (M) (28), a higher M requiring a lower induction time, hence a fluid strain. Thus a critical shear strain (at constant shear rate) or a critical shear rate (at a constant shear strain) is a precondition for these effects to occur. On the other hand, the critical shear rate for accelerated crystallization shifts to a lower value as molecular weight increases. This is due

to underlying molecular relaxation processes. Keller and Klonaar (3) have proposed the following relationship in the case of elongational flow induced crystallization:

$$\dot{\epsilon}_c \propto M^{-\beta} \quad (3)$$

where, $\dot{\epsilon}_c$ is the critical elongational rate, M is the critical molecular weight and β is a factor, which was found to be equal to 1.5 in their experiments with polyethylene solutions. The critical elongation rate is associated to the coil-extended chain transition of the polymer molecules in the solution under flow.

Following Keller's observations in elongational flow experiments, we propose a similar behavior to explain the shear flow induced crystallization experiments. At a given shear rate only those molecules having a chain length (molecular weight) above a critical value (critical orientation molecular weight) can form stable oriented row-nuclei. When the polymer melt, containing a broad chain length distribution (molecular weights) is subjected to a shear flow field of a particular $\dot{\gamma}$, only the longest chains will be extended with a low end cut-off at the critical orientation molecular weight (M^*), while the rest of the molecules will remain unstretched. The result is a bimodal distribution of chain molecules represented by a double population of stretched and unstretched chains with no intermediate stage between them. Increasing $\dot{\gamma}$ does not increase the chain extension substantially but increases the amount of material that becomes

extended by increasingly 'cutting into' the distribution from the high molecular tail downwards (see Figure 11). A typical MWD curve for a polymeric material is shown in Figure 11. The "critical orientation molecular weight" (M^*) on the curve shifts to a higher value at low deformation rates as shown by lines 1 (low $\dot{\gamma}$) and 2 (high $\dot{\gamma}$). The area under the MWD curve represents the fraction of the material having molecules above the critical orientation molecular weight. If we Assume that a relationship between M^* and $\dot{\gamma}$ applies then:

$$M^* \propto \dot{\gamma}^{-\hat{\alpha}} \quad (4)$$

$$M^* = K \dot{\gamma}^{-\hat{\alpha}} \quad (5)$$

$$F(\dot{\gamma}) = M^* / K = \dot{\gamma}^{-\hat{\alpha}} \quad (6)$$

where M^* is the critical orientation molecular weight, $\dot{\gamma}$ is the shear rate and K is the proportionality constant and $\hat{\alpha}$ is the exponent of $\dot{\gamma}$. The value of the $\hat{\alpha}$ constant is not known, however we can examine the nature of the M^* versus $\dot{\gamma}$ variation for various values of $\hat{\alpha}$. Figure 12 shows the calculated profiles of the function $F(\dot{\gamma})$ (equation 6) for several $\hat{\alpha}$ values. From these curves it is seen that *[Note: The M^* value is different from the conventional critical molecular weight used in the rheology, but may be related with it.]*

the value of M^* is more sensitive at low shear rates than at high shear rates, reaching a plateau at high shear rates.

The calculated values of the oriented fraction in the i-PP polymer bulk after deformation and subsequent crystallization can be assumed to be proportional to the fraction of the MWD above the critical orientation molecular weight. From the GPC chromatogram for the isotactic polypropylene resin and the calculated values of the oriented fraction (see note below) for various shear rates, the critical orientation molecular weight values corresponding to each shear rate were determined. Figure 13 shows the estimated M^* values for the three shear rates studied. The values of the parameters K ($= 657000$) and β ($= 0.15$) in equation 5 were obtained by fitting the experimental data. According to Figure 13 the critical orientation molecular weight, M^* (~ 300000), does not seem to vary significantly above the shear rate of 60 s^{-1} .

Analysis of the experimental data using equation 4, explains why no significant variation in the oriented fraction was observed at the shear rate of 57 and 102 s^{-1} . As pointed out above, at low $\dot{\gamma}$ values only the longest chains, having highest relaxation times and entanglements, will be extended, with a low cut-off end at the critical orientation M^* value (line 1 in Figure 11). As $\dot{\gamma}$ is increased, the population of polymer molecules having lower molecular weight values (lower relaxation time and entanglements) than the longest chains can *[Note: we acknowledge that the oriented fraction value contains both stretched chains or row-nuclei as well as transcrystallites that are oriented.]*

become extended and, thus, increasingly 'cutting into' the distribution from the high molecular tail downwards (line 2 in Figure 11).

In practice, the process cannot continue indefinitely. In fact the relaxation time for the shortest chains is high and has few or no entanglements, and cannot form long-lived extended structures. Thus, there is a limiting value for the critical orientation molecular weight above which the stable oriented structures can be only formed even at high values of shear rates. It should be noted that the K and β parameters in equation 4 have been calculated for the step shear condition in which the strain (1428 %) was kept constant. Both, the total strain and the shear rate affect the coil to stretch transition in a shear flow field. Further experimental results are required to understand the effect of the total strain. The calculated values of the parameters, K , β , and M^* are based on three experimental data points and therefore must be used with caution.

Conclusions

- 1) The SAXS patterns of isotactic polypropylene melt at 140 °C show the development of oriented crystallites upon application of the step shear at 1428% strain and shear rates of 10, 57, and 102 s⁻¹. Results suggest that the long chain i-PP molecules orient and align in the flow direction and form microfibrillar structures, which enhance nucleation and subsequent growth of the oriented crystalline lamellae.

- 2) Due to the imposed step shear the crystallization kinetics of isotactic polypropylene increases by two orders of magnitude as compared to quiescent crystallization.
- 3) The fraction of oriented crystallites in the polypropylene bulk is lower at the shear rate of 10 s^{-1} as compared to the oriented fraction at the shear rates of 57 and 102 s^{-1} .
- 4) No significant difference in the oriented fraction was observed at the shear rates of 57 and 102 s^{-1} . This "unexpected" observation is related to the critical orientation molecular weight (M^*). Under the imposed shear (or elongational) flow conditions only polymer molecules having a molecular weight above a critical orientation molecular weight can form microfibrils and oriented structures.
- 5) In analogy with Keller's observations in diluted systems, the relationship between the critical orientation molecular weight and the shear rate (at constant strain); ($M^* \text{ vs } \dot{\gamma}^{-\beta}$), has been used to calculate the critical orientation molecular weight values at different shear rates.
- 6) The critical orientation molecular weight is a very sensitive quantity at low shear rates and reaches a plateau above a shear rate of 60 s^{-1} . At the shear rates of 57 and 102 s^{-1} the value for the fraction of oriented material does not vary significantly.
- 7) The step shear experiment using the modified Linkam shear stage provides a technique in which, both, the shear rate and the shear strain can be varied independently.

Acknowledgements

We wish to record our appreciation to the late Prof. Andrew Keller and to Prof. Richard S. Stein, and Dr. J. Kornfield for helpful discussions and interpretations of the results. We express our thanks to the US-Spain Science & Technology Program 1999 for the generous support of this joint research project. The financial support for this work has been also partly provided by NSF DMR-97 and by DGICYT, Spain (grant PB-0049) and ExxonMobil.

Legend to Figures

Figure 1. Schematics of the Linkam Shear stage and the small angle x-ray scattering setup.

Figure 2. Schematics of the shear profile across the sample thickness.

Figure 3. Schematics of the temperature profile and the step shear during the experiments

Figure 4. SAXS patterns of i-PP at 140 °C before and after step shear (Shear rate = 102 s⁻¹, Strain = 1428 %).

Figure 5. Deconvolution procedure of the scattering due to the oriented and unoriented species: a) original SAXS image, b) isotropic component, c) oriented component.

Figure 6. Time evolution of: A) total scattered intensity, B) scattered intensity from the unoriented scatterers, and C) scattered intensity from the oriented scatterers after the step shear.

Figure 7. Fraction of oriented material and half-time of crystallization as a function of shear rate in i-PP at 140 °C.

Figure 8. Model of structure development: a) before shear, b) at short time (<100 s) after the step shear, c) at longer time after the step shear.

Figure 9. Development of the oriented structure in i-PP after the step shear.

Figure 10. Crystallization kinetics in i-PP at 140 °C after the step shear.

Figure 11. Schematics showing the critical orientation molecular weight at low and high shear rates.

Figure 12. Calculated profiles of the function $F(\dot{\gamma})$ for various values of the exponent β in equation 5.

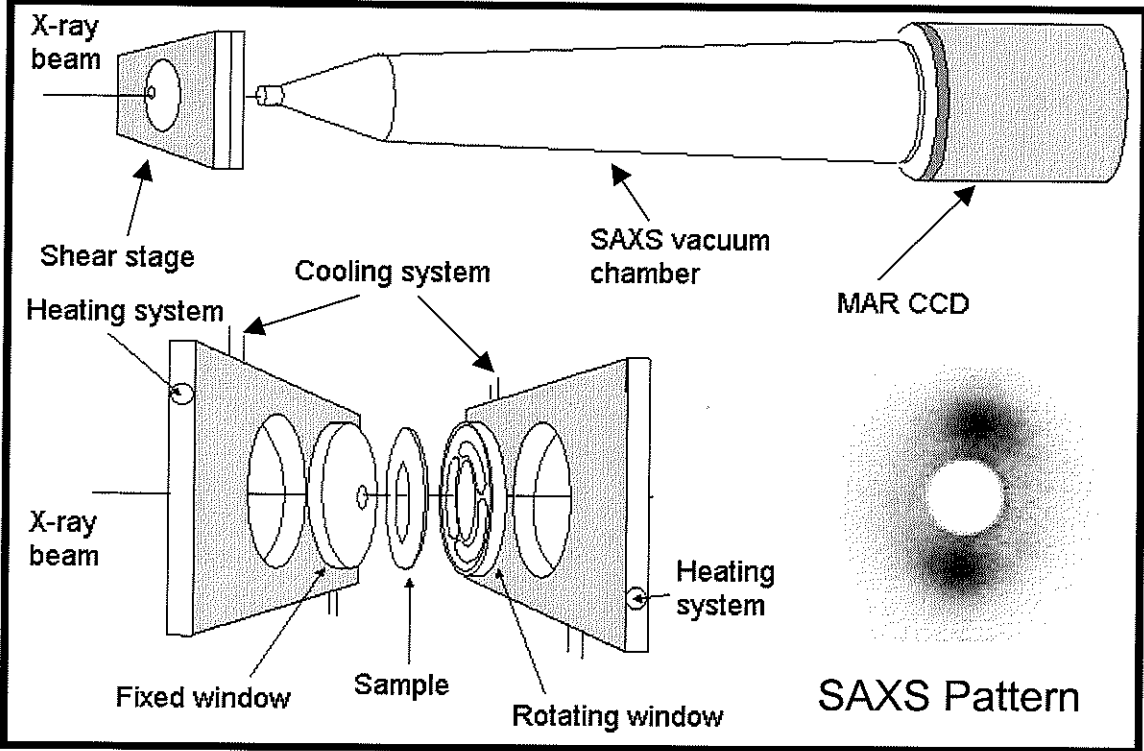
Figure 13. Critical orientation molecular weight as a function of shear rate for i-PP at 140 °C under the step shear using 1428% strain (the solid line is the regression fit of the experimental data).

References

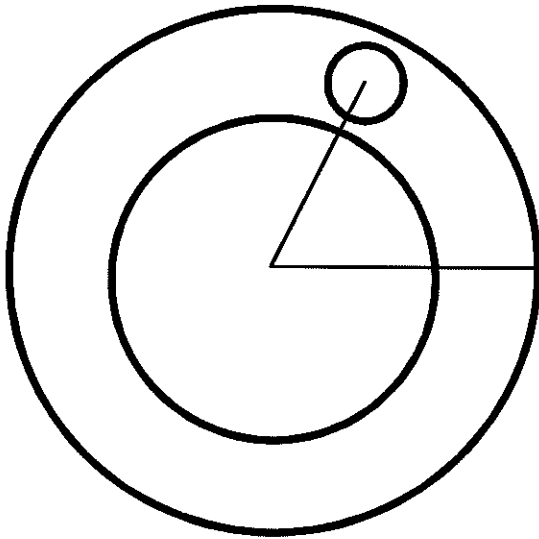
1. Lee, O.; Kamal, M. R., *Polym. Eng. Sci.*, **1999**, 39(2), 236.
2. Pennings, A. J.; Van der mark, J. M. A.; Booij, H. C., *Kolloid. ZZ. Polym.*, **1970**, 236, 99.
3. Keller, A.; Kolnaar, H. W. H., *Processing of Polymers*, ed. Meijer, H. E. H., Vol. 18, Chapter 4, 189-268, **1997**.
4. Jerschow, P.; Janeschitz-Kriegl, H., *Inter. Polym. Process.*, **1997**, 12 (1), 72.
5. Jerschow, P.; Janeschitz-Kriegl, H., *Rheo. Acta*, 35, 1996, 127-133.
6. Liedaur, S.; Eder, G.; Janeschitz-kriegl, H., *Intern. Polym. Process.*, **1995**, 10(3), 243.
7. Liedauer, S.; Eder, G.; Janeschitz-Kriegl, Jerschow, P.; Geymayer, W.; Ingolic, E., *Inter. Polym. Process.*, **1993**, 8 (3), 236.
8. Kumaraswamy, G.; Issaian, A. M.; Kornfield, J. A., *Macromolecules*, **1999**, 32 (22), 7537.
9. Kumaraswamy, G.; Varma, R. K.; Issaian; A. M.; Kornfield, J. A.; Yeh, F.; Hsiao, B. S., *Polymer*, accepted, **2000**.
10. Bayer, R. K.; Eliah, A. E.; Seferis, J. C., *Polym. Eng. Rev.*, **1984**, 4, 201.
11. Ania, F.; Bayer, R. K.; Tschmel, A.; Michler, H. G.; Naumann, I.; Baltá Calleja, F. J., *J. Mater. Sci.*, **1996**, 31, 4199.
12. Rueda, D. R.; Ania, F.; Baltá Calleja, F. J., *Polymer*, **1997**, 38 (9), 2027.
13. Haas, T. W.; Maxwell, B., *Polym. Eng. Sci.*, **1969**, 9, 225.
14. Kobayashi, K.; Nagasawa, J.; *J. Macromol. Sci., Phys. B*, **1970**, 4 (2), 331.
15. Wereta, A.; Gogos, C., *Polym. Eng. Sci.*, **1971**, 11, 19.

16. Krueger, D.; Yeh, G. S. Y., *J. Appl. Phys.*, **1972**, 43, 4339.
17. Fritzsche, A. K.; Price, F. P., *Polym. Eng. Sci.*, **1974**, 14, 401.
18. Tan, V.; Gogos, C., *Polym. Eng. Sci.*, **1971**, 11, 512.
19. Lagasse, R. R.; Maxwell, B., *Polym. Eng. Sci.*, **1976**, 16, 189.
20. Fritzsche, A. K.; Price, F. P., Ulrich, R. D., *Polym. Eng. Sci.*, **1976**, 16, 182.
21. Ulrich, R. D.; Price, F. P., *J. Appl. Polym. Sci.*, **1976**, 20, 1077.
22. Tribout, C.; Monasse, B.; Haudin, *Coll. Polym. Sci.*, **1996**, 274, 197.
23. Kalay, G.; Bevis, M. J., *J. Polym. Sci., Polym. Phys.*, **1997**, 35, 265.
24. Huang H., *J. Appl. Polym. Sci.*, **1998**, 67, 2111.
- 24^a. Wilkinson, A.N. & Ryan, A.J., "Polymer processing and Structure Development", Kluwer, Dodrecht, **1998**
25. Varga, J., *J. Mater. Sci.*, **1992**, 27, 2557.
26. Varga, J.; Karger-Kocsis, J., *J. Polym. Sci., Part B, Polym. Phys.*, **1996**, 34 (4), 657.
27. Kargin, V. A.; Andrianova, G. P., *Dokl. Akad. Nauk. USSR*, **1962**, 146, 1337.
28. Binsbergen, F. L., *Nature*, **1966**, 211, 516.
29. Thomason, J. L.; Van Rooyen, A. A., *J. Mater. Sci.*, **1992**, 27, 897.
30. Misra, S.; Lu, F. M.; Spruiell, J. E.; Richeson, G. C., *J. Appl. Polym. Sci.*, **1995**, 56, 1761.
31. Vleeshouwers, S.; Meijer, H. E. H., *Rheol. Acta*, **1996**, 35, 391.
32. Moitzi, J.; Skalicky, P., *Polymer*, **1993**, 34 (15), 3168.
33. Haudin, F. J.; Monasse, B., *J. Mater. Sci.*, **1999**, 34, 2089.
34. Wunderlich, B., *Macromolecular Physics*, Academic, New York, Vol. 2, **1973**.

35. Jerschow, P.; Janeschitz-Kriegl, H., *Rheo. Acta*, **1996**, 35, 127-133.
36. White, H. M.; Bassett, D. C., *Polymer*, **1997**, 38(22), 5515.
37. Ran, S.; Zong, X.; Fang, D.; Hsiao, B.; Chu, B.; Ross, R., *J. Appl. Crystallography*, *accepted*, **2000**.
38. Goschel, U.; Swartjes, F.H.M.; Peters, G.W.M.; Meijer, H.E.H., *Polymer*, **2000**, 41 (4), 1541.

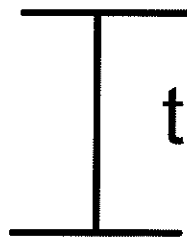
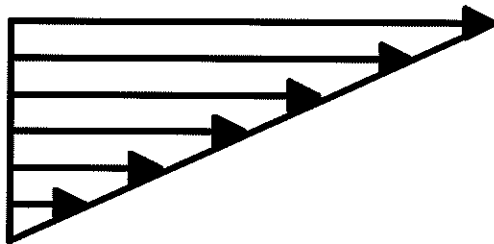


x-ray window



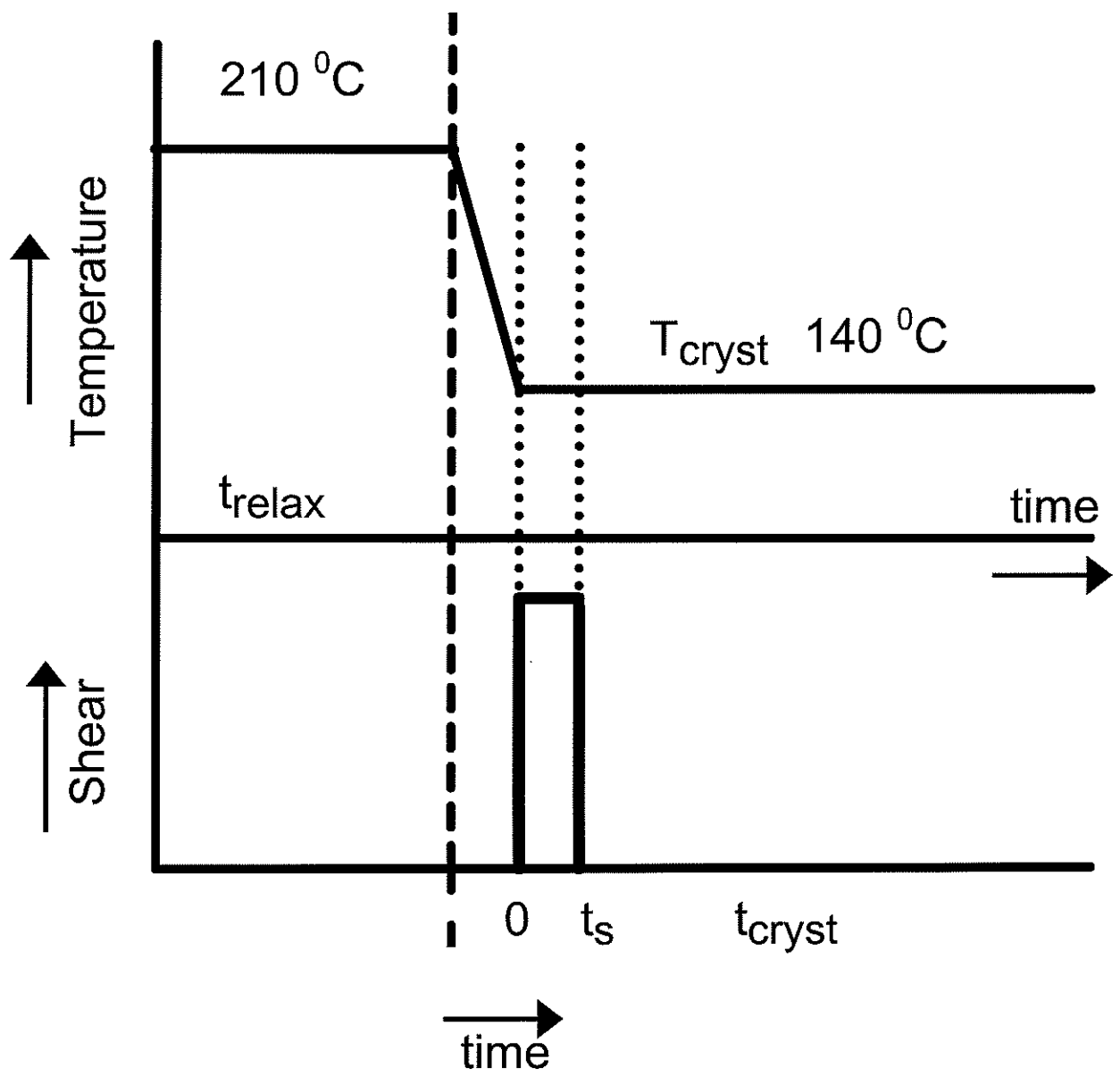
Max shear

Bottom



Zero shear

Top



Figure

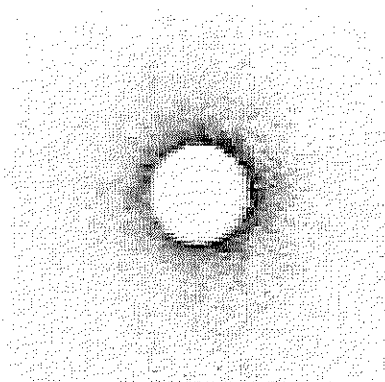


Fig 4a -
Amorphous melt
($t = 0$), No shear

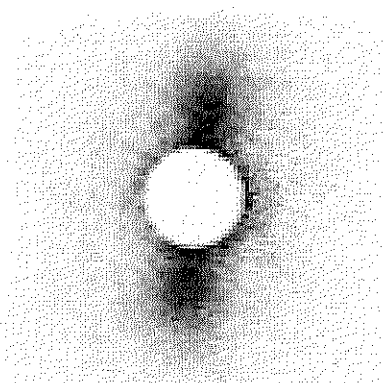


Fig 4b -
 $t = 120$ s
after shear

Flow
direction

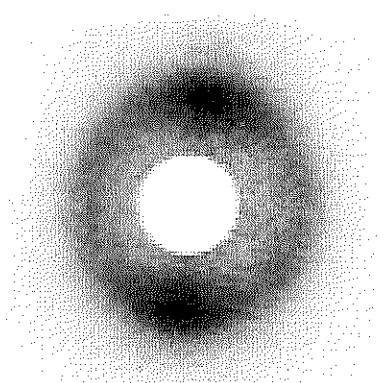



Fig 4c
 $t = 900$ s
after shear

Figure 5

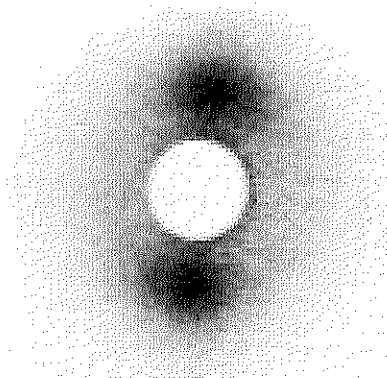


Fig 5a
SAXS
image

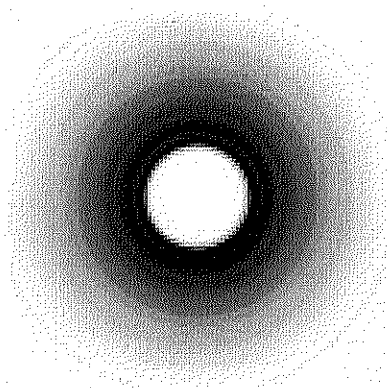


Fig 5b
Isotropic
component

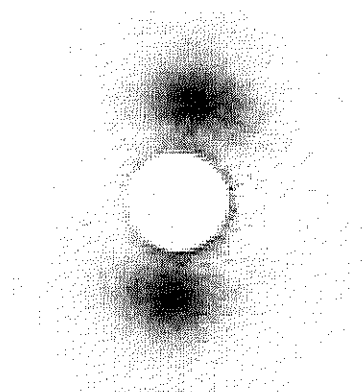


Fig 5c
Oriented
component

Figure 6

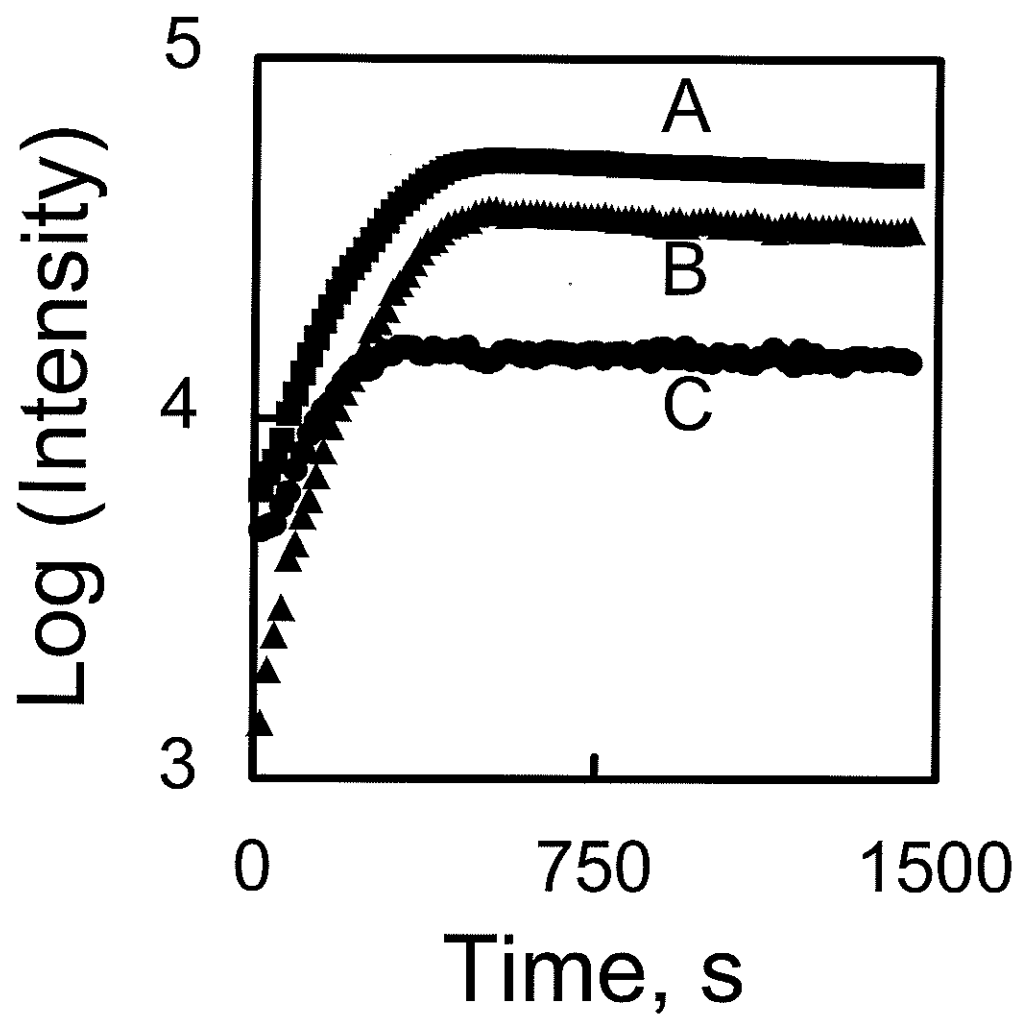
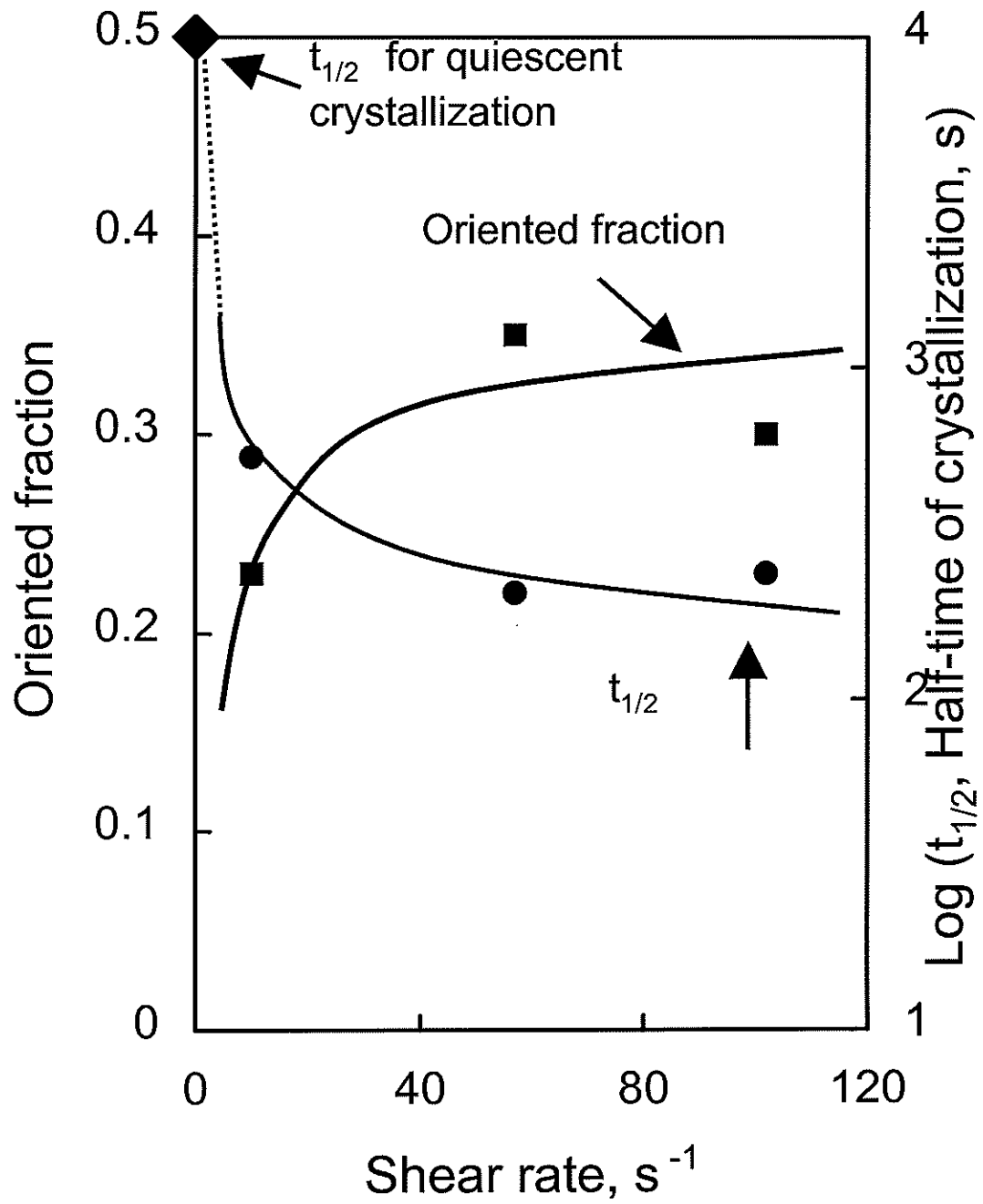
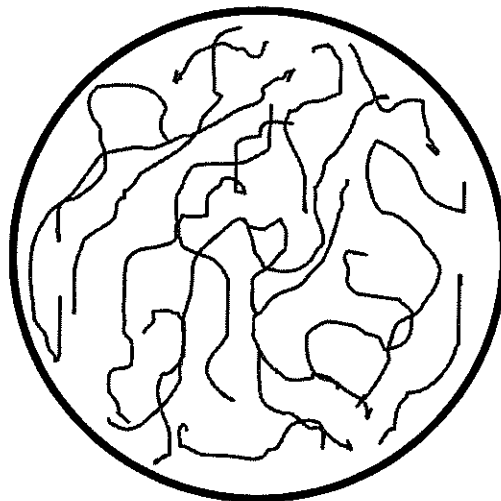


Figure 7



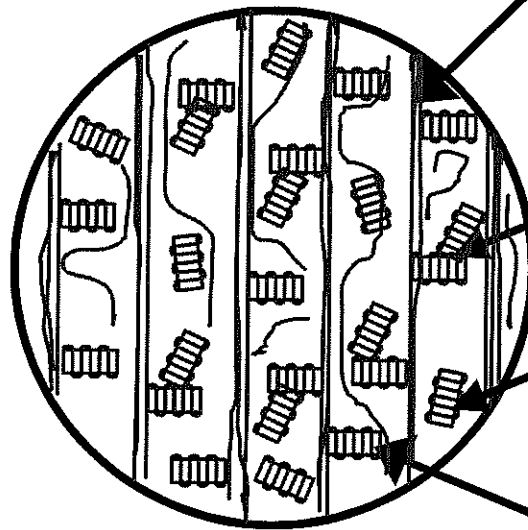
Figure

Fig 8a



Amorphous melt

Fig 8b



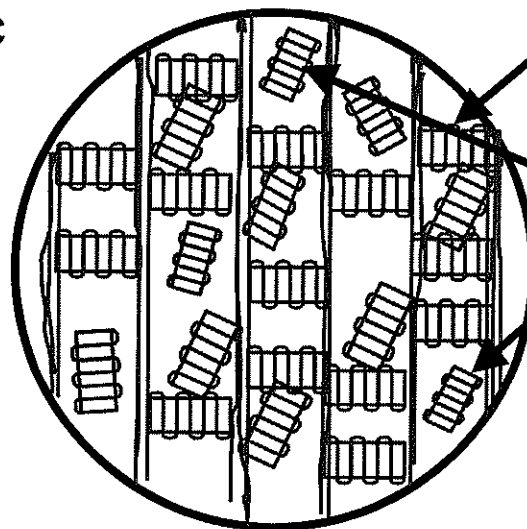
Extended Fibril structure

Transcrystalline structures

Unoriented crystals

Folded chain crystals

Fig 8c



Unoriented crystals



Flow direction

Figure

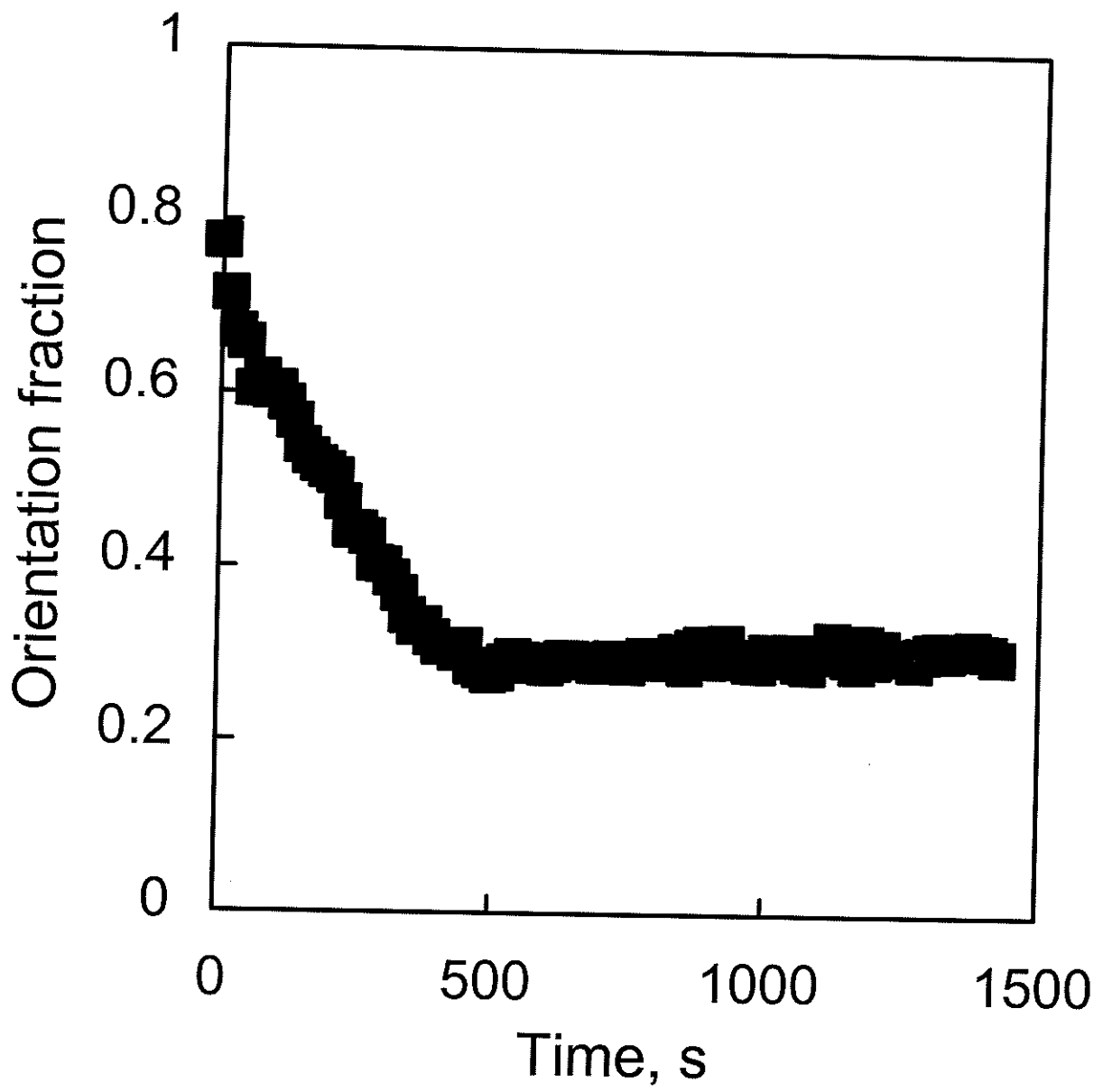


Figure 10

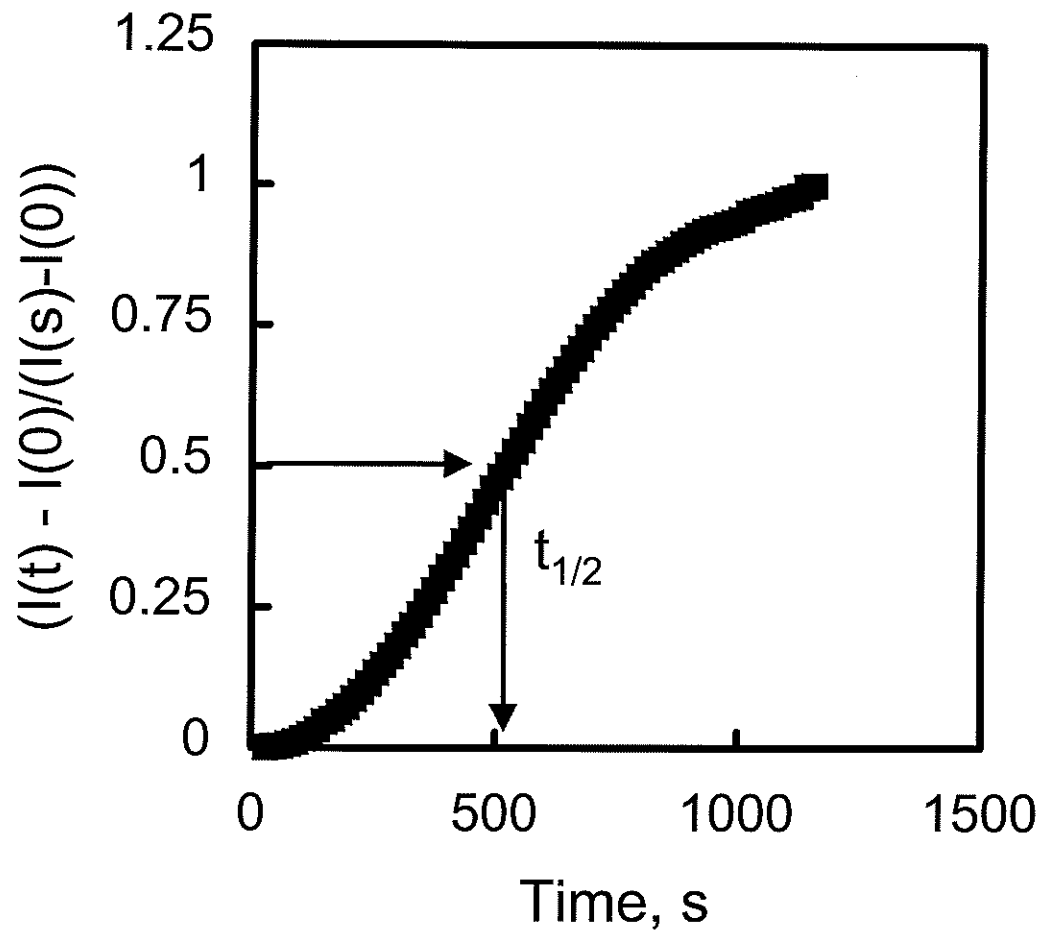


Figure 11

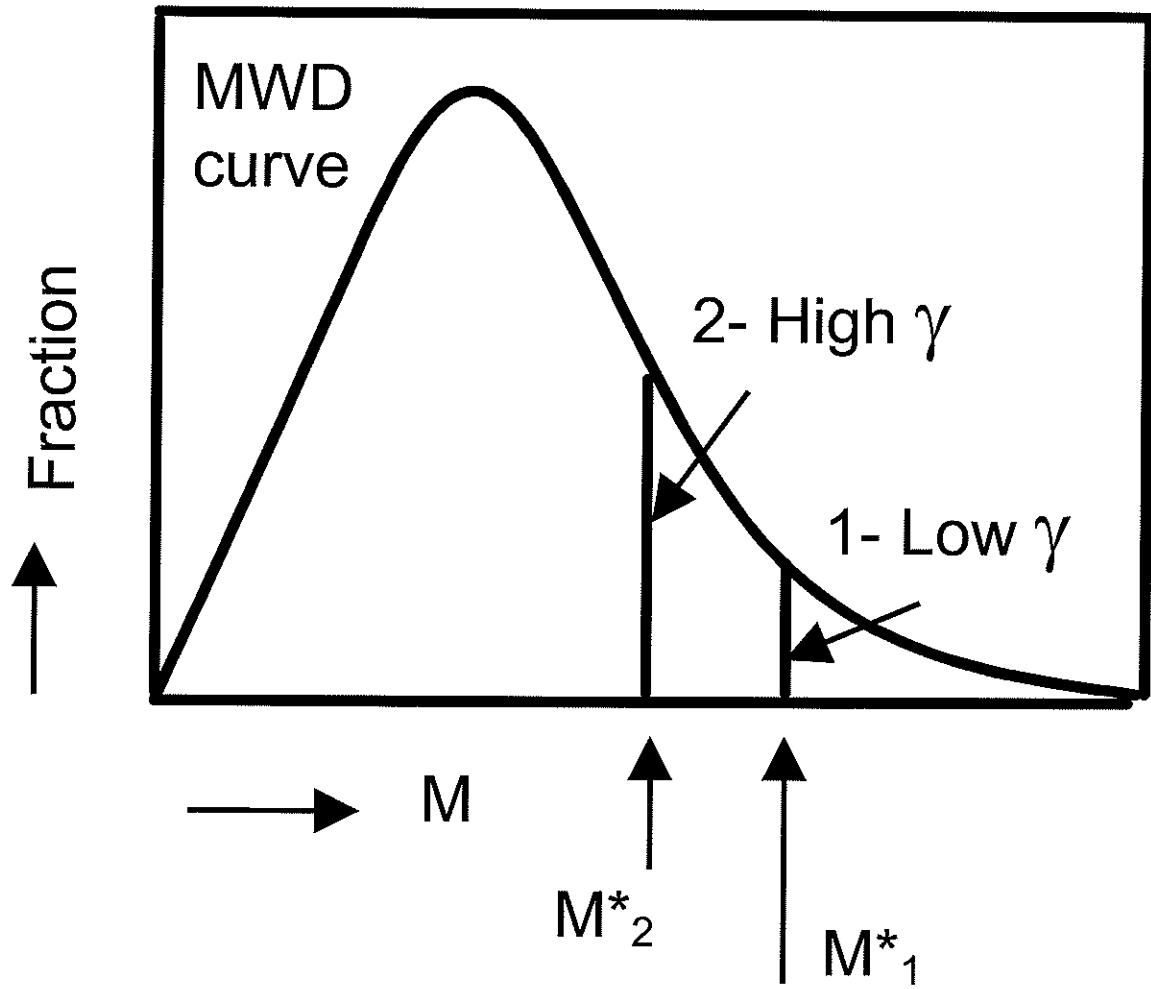


Figure 12

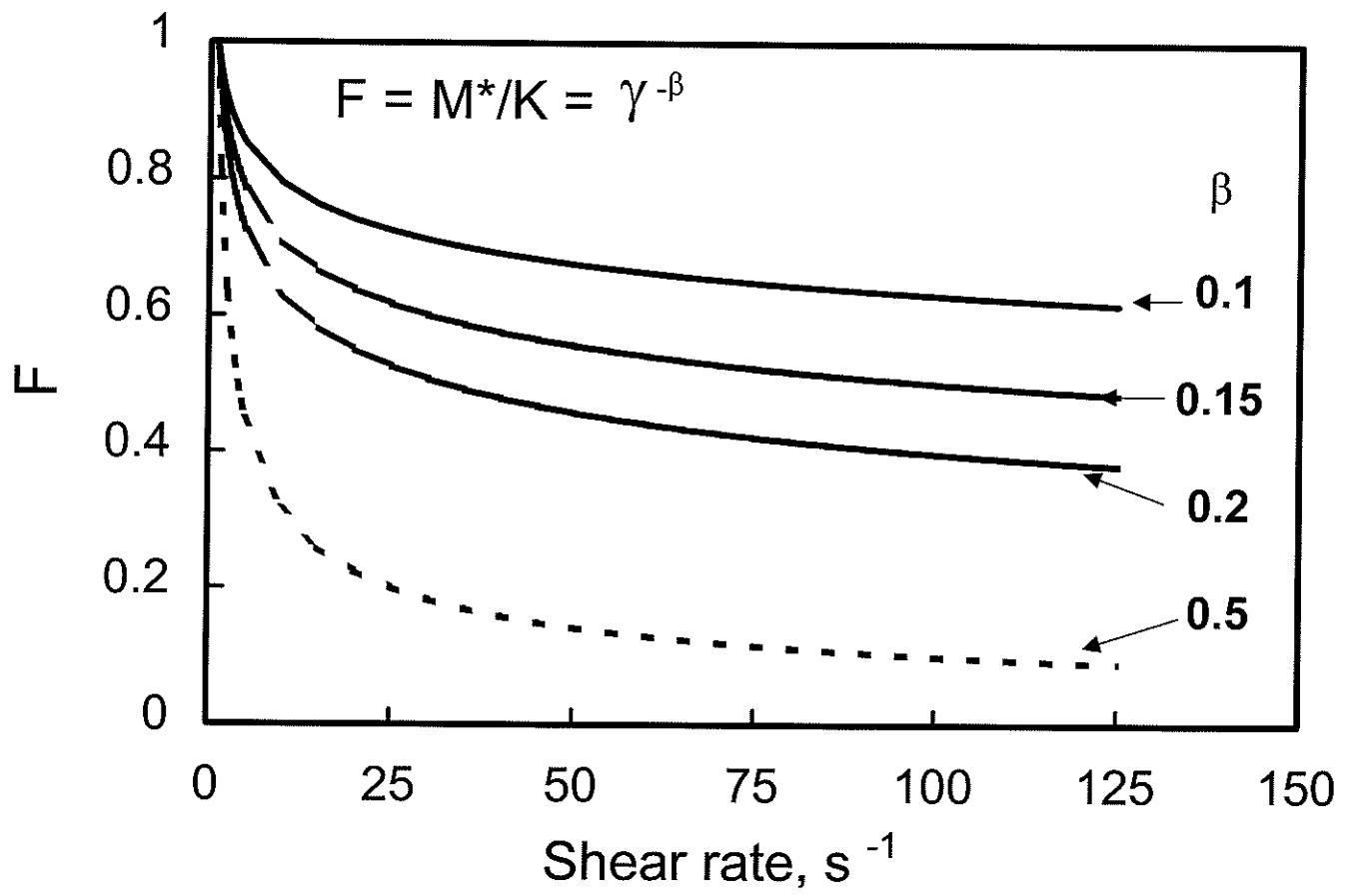
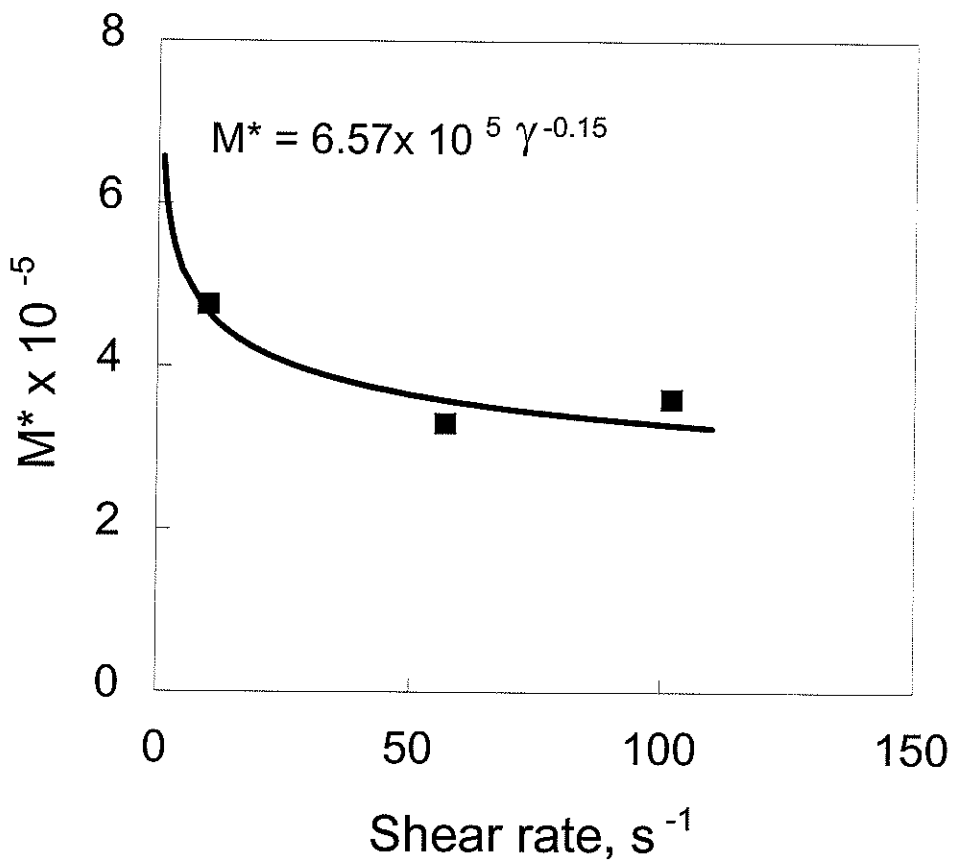
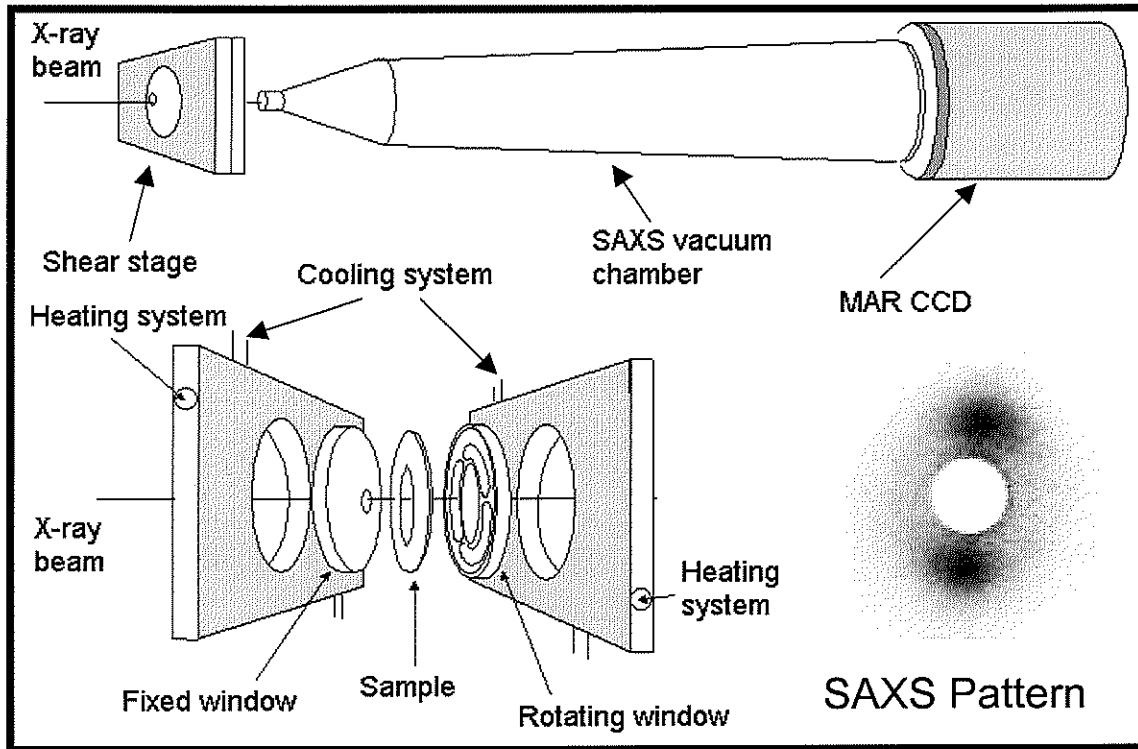
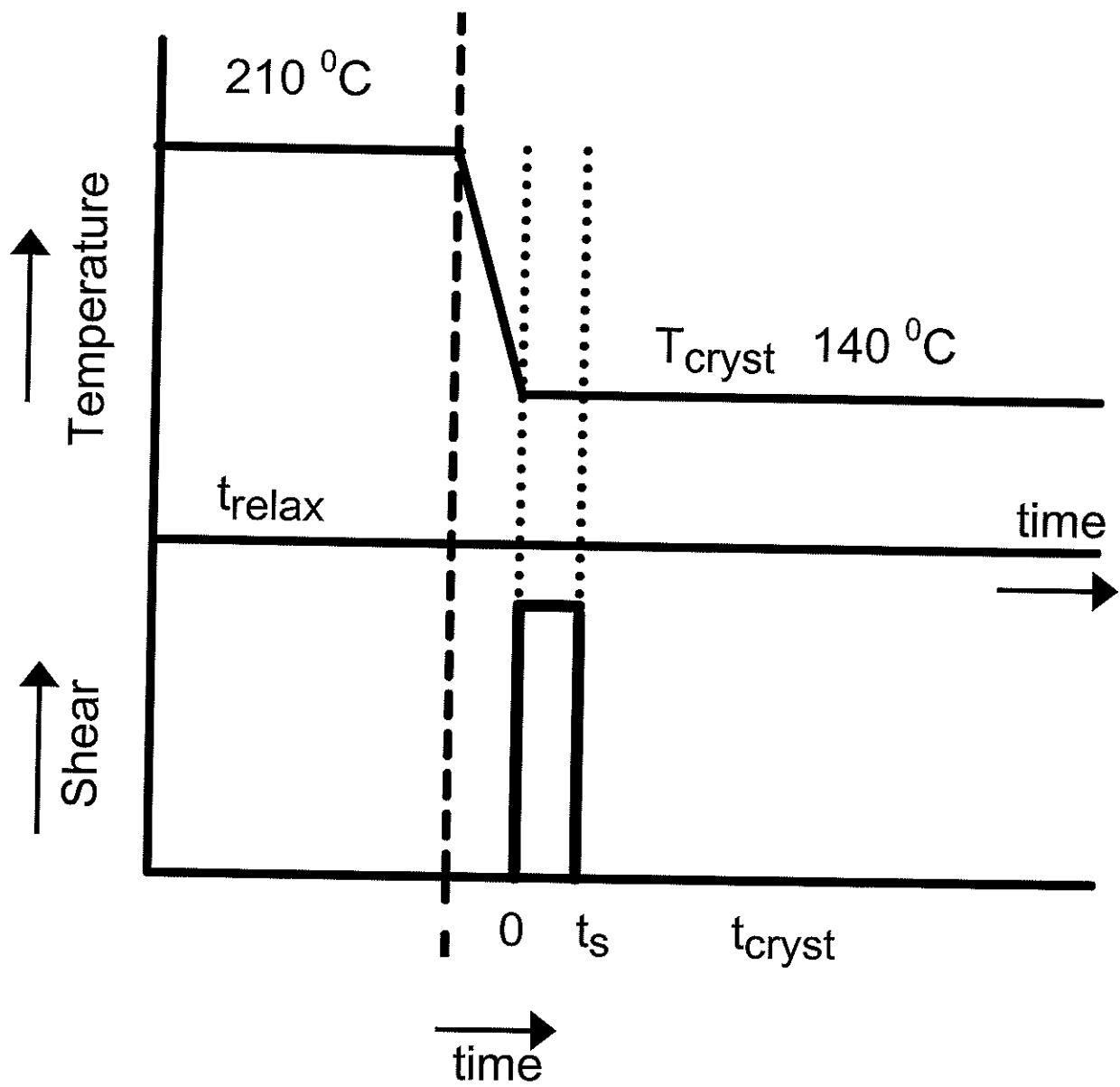


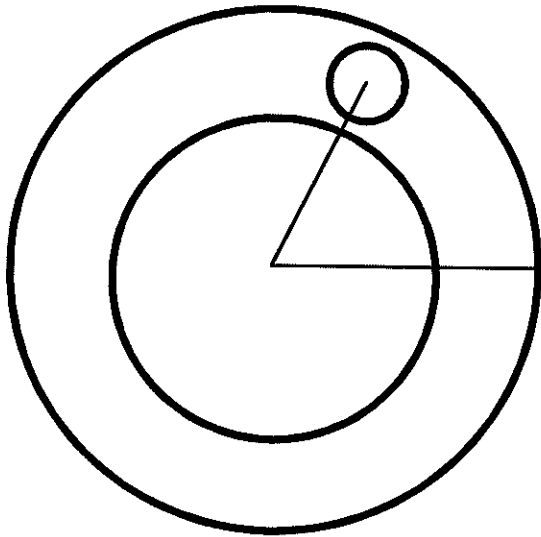
Figure 13





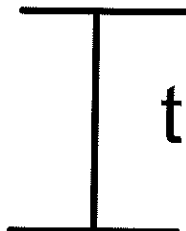
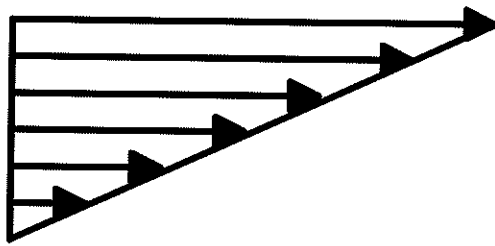


x-ray window



Max shear

Bottom



Zero shear

Top